

Supporting Information for

**A continuum membrane model can predict curvature sensing by helix
insertion**

Yiben Fu¹, Wade F. Zeno², Jeanne C. Stachowiak³, Margaret E. Johnson^{1*}

¹T. C. Jenkins Department of Biophysics, The Johns Hopkins University, 3400 N. Charles St., Baltimore, Maryland 21218, USA

²Mork Family Department of Chemical Engineering and Materials Science, The University of Southern California, Los Angeles, California, 90089, United States

³Department of Biomedical Engineering, The University of Texas at Austin, Austin, Texas 78712, United States

**Corresponding Author:* margaret.johnson@jhu.edu

Supporting Figures:

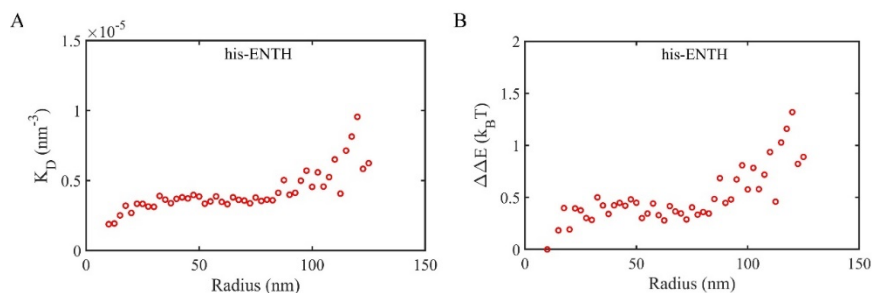


Figure S1. Binding of ENTH without its amphipathic helix present is insensitive to curvature. (a) Experimental surface coverage measurements of the hexa-histidine tag ENTH (his-ENTH) that lacks the amphipathic helices are converted to dissociation constants as described in the main text. (b) The corresponding membrane energy change is nearly flat, due to the curvature insensitivity across all vesicle sizes. The solution concentration of the his-ENTH experiment is 25 nM.

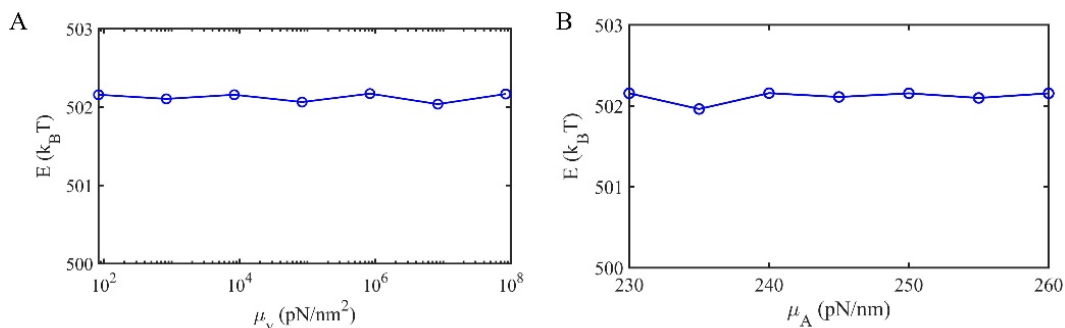


Figure S2. Influence of the osmotic pressure and the membrane area elasticity on membrane energy changes. (a) Changes to the volume constraint coefficient, μ_V , reflecting changes in osmotic pressure, do not cause discernable changes in the membrane energy following insertion. $\mu_A = 250$ pN/nm. (b) Changes to the area elasticity μ_A similarly do not impact the membrane energy change following insertion. $\mu_V = 83.4$ pN/nm². The size of the vesicle is $R = 14$ nm, the insertion size is 2 nm² (Fig 1), with $c_0^{\text{ins}} = 0.1$ nm⁻¹.

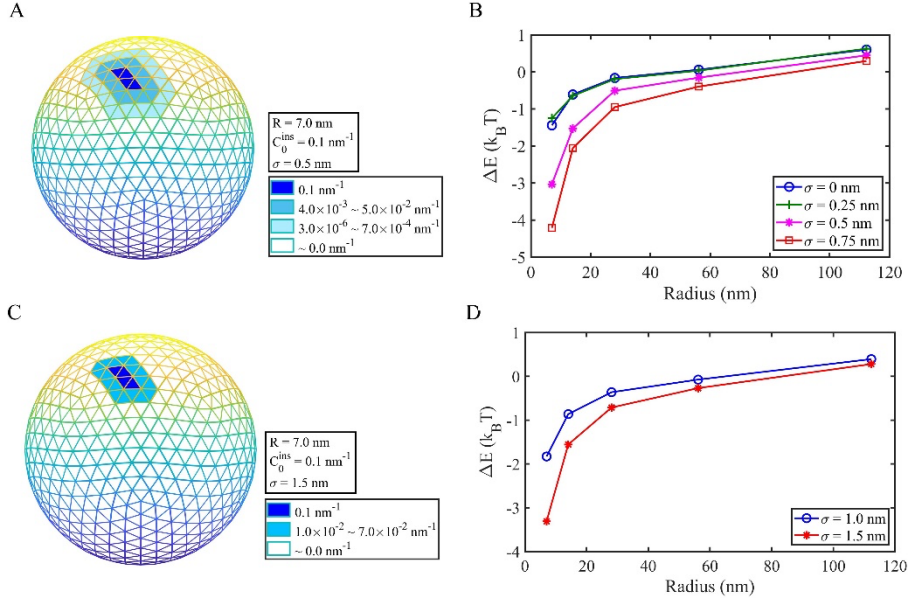


Figure S3. Expanding the perturbed area due to the insertion amplifies the changes in membrane energy. (A-B) Expanding the perturbed area due to insertion using a Gaussian function. (A) Here, the insertion is still modeled as occupying an area of 2 nm^2 , with a spontaneous curvature of $c_0^{\text{ins}} = 0.1 \text{ nm}^{-1}$ (dark blue triangles). In addition, the membrane directly around the insertion is also modeled as having a non-zero spontaneous curvature, decaying with distance according to a Gaussian distribution with $\sigma = 0.5 \text{ nm}$. Teal triangles thus have a lower but non-zero value of $c_0^{\text{ins}}(x) \sim 0.004\text{-}0.05 \text{ nm}^{-1}$. Lighter blue triangles have $c_0^{\text{ins}}(x) \sim 3 \times 10^{-6}\text{-}7 \times 10^{-4} \text{ nm}^{-1}$, and the remaining surface has zero spontaneous curvature. (B) As we increase the spread of the insertion perturbation to larger distances (increased σ), we see larger responses in the membrane energy change. The results for $\sigma = 0$ change only the spontaneous curvature of the helix-containing triangles, and are thus identical to the original model. (C-D) Expanding the perturbed area as a linear function. (C) The insertion can be modeled as impacting the spontaneous curvature of neighboring membrane, in a distance-dependent way, $c_0^{\text{ins}}(x) = c_0^{\text{ins}} [(x - x_0)/\sigma + 1]$, where x is the distance to the insertion zone center x_0 , and σ is the width of the spread. (D) As the spread of the insertion region is increased (increased σ), we see larger responses in the membrane energy change. $c_0^{\text{ins}} = 0.1 \text{ nm}^{-1}$ and $\kappa = 20 k_B T$.

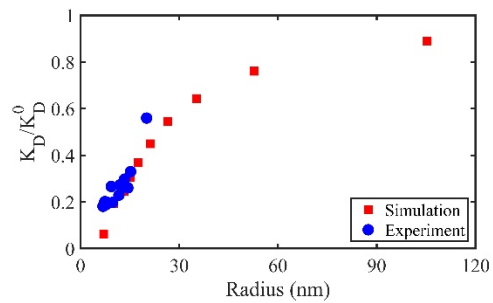


Figure S4. Curvature sensing of ENTH on the cylinder membrane. The experiment data of the dissociation constant K_D as the cylinder radius changes is the same as Fig 7B, or see Fig 2E in ref. [16].

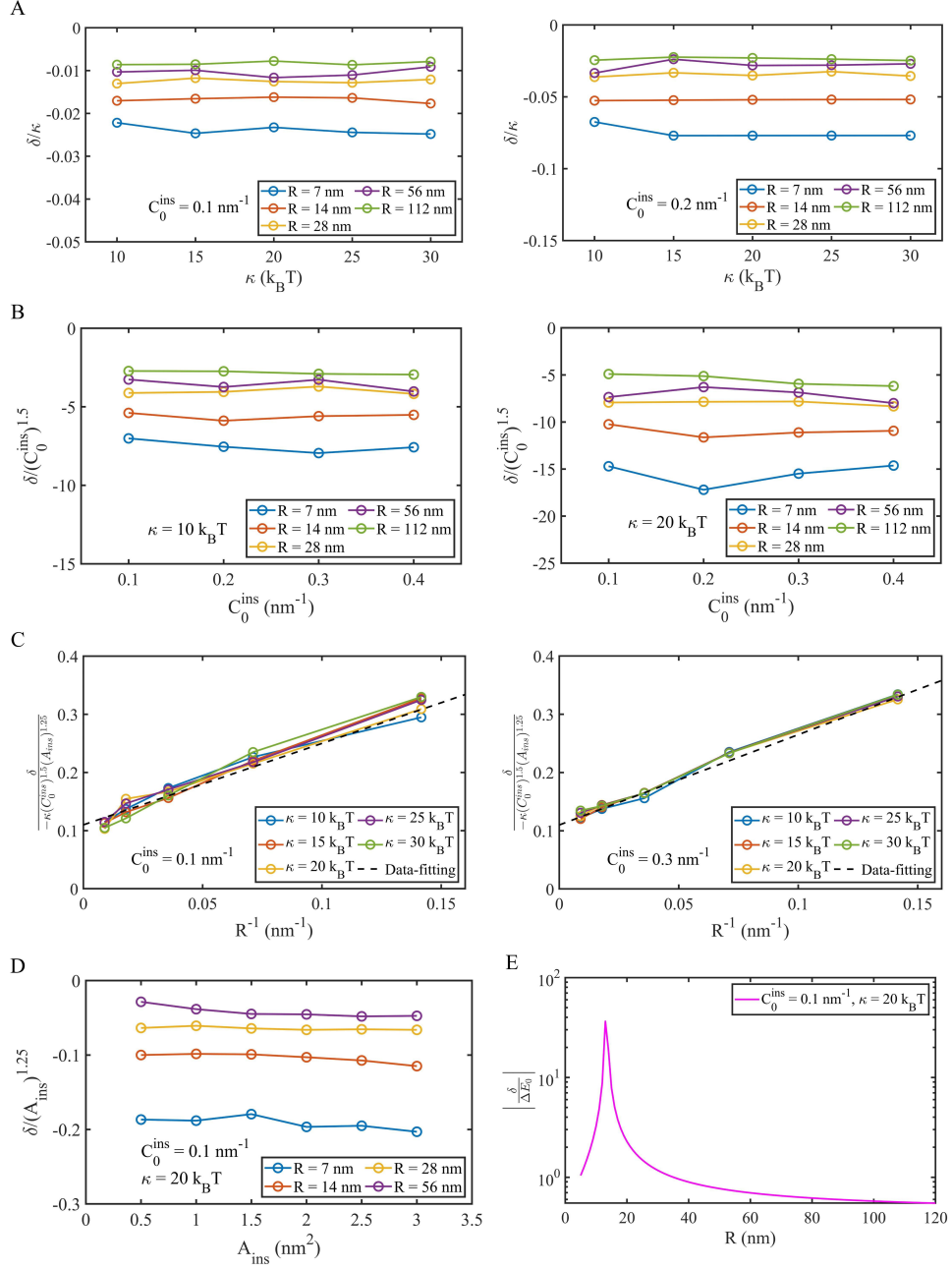


Figure S5. Dependence of the membrane shape change energy, δ , with variations to membrane and insertion parameters (R , c_0^{ins} , κ , and A_{ins}). Based on the comparisons of the numerical δ values with variations in R , c_0^{ins} , κ , and A_{ins} , we ultimately end up with an empirical fit function $\delta(R, c_0^{\text{ins}}, \kappa, A_{\text{ins}}) = -\kappa c_0^{\text{ins}n} A_{\text{ins}}^m \left(\frac{p}{R} + q\right)$, with 4 fit parameters n , m , p , and q , where only q has dimensions, which match the units of R^{-1} .

The sum of n and m is also constrained to cancel out units with R^{-1} , such that $2m - n - 1 = 0$. (A) Our data show that $\delta \propto \kappa$ regardless of variation in other parameters. (B) Our data show that $\delta \propto (c_0^{\text{ins}})^n$. By performing non-linear fitting, we find that $n = 1.50 \pm 0.10$. All errors reported here are standard errors. (C) Our data show that $\delta \propto R^{-1}$. To define the final two fit parameters, we compare $\delta / (-\kappa c_0^{\text{ins}n} A_{\text{ins}}^m)$ to R^{-1} , having already fixed n and m , as shown by the y-axis rescaling of δ . Linear fitting then gives a slope 1.51 ± 0.11 and y-intercept 0.11 ± 0.008 , and thus we have that $p = 3/2$ and $q = 0.1 \text{ nm}^{-1}$. (D) Our data show that $\delta \propto (A_{\text{ins}})^m$, where non-linear fitting gives $m = 1.25 \pm 0.026$. (E) Lastly, we find that the magnitude of δ is typically comparable to the energy change due to the insertion, ΔE_0 , but makes a 10-fold larger contribution for small to intermediate vesicles of a curvature similar to the size of c_0^{ins} .

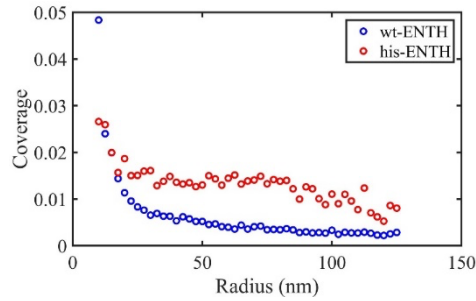


Figure S6. Experimentally measured surface coverage of ENTH on vesicles. The coverage is defined as $N\pi r^2 / (4\pi R^2)$, where N is the copy number of ENTH bound on the vesicle, $r = 2 \text{ nm}$ is the ENTH size and R is the vesicle radius.

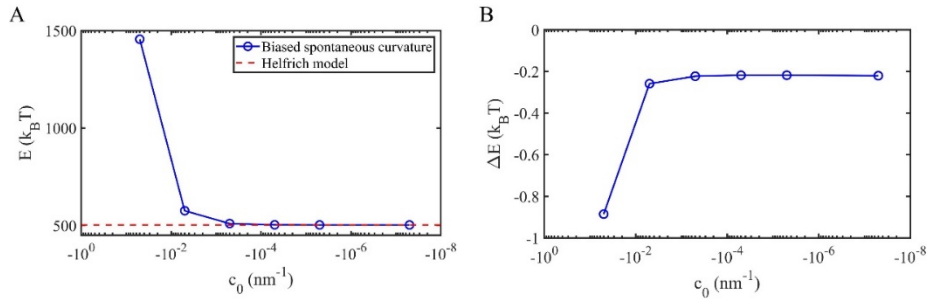


Figure S7. Influence of the biased initial membrane spontaneous curvature on the membrane energy calculation. The membrane composition here in experiments is mainly POPC ($\sim 90\%$ of total lipids). POPC has a negative spontaneous curvature about -0.05 nm^{-1} , which means it should prefer the inner leaflet of the small unilamellar vesicle. Since lipid rearrangement occurs between the bilayers, some POPC lipids will flip into the inner layer from the outer layer, which will make the bilayer spontaneous curvature larger than

-0.05 nm^{-1} . Therefore, we ran some simulations with the spontaneous curvature value -0.05 nm^{-1} . (A) Membrane energy of the spherical vesicle as a function of initial membrane spontaneous curvature. The Helfrich model gives $E = 8\pi\kappa$. (B) The membrane energy change due to one protein insertion. $R = 28 \text{ nm}$, $\kappa = 20 k_B T$.

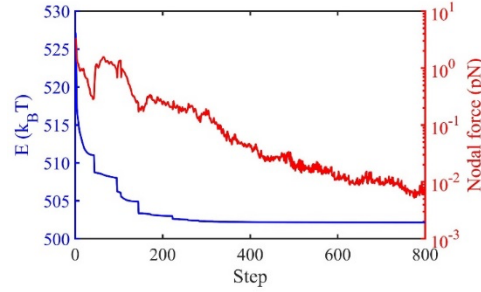


Figure S8. Energy minimization of the continuum membrane model following insertion. Simulation results from a vesicle with $R = 14 \text{ nm}$ and one insertion on the surface, $c_0^{\text{ins}} = 0.1 \text{ nm}^{-1}$, $\kappa = 20 k_B T$.

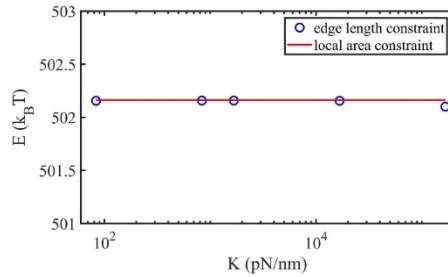


Figure S9. Membrane energy following insertion is not sensitive to constraint choice on insertion region. For the edge length constraint method, we tried five different values of K . For the local area constraint method, we used $\mu_A = 250 \text{ pN/nm}$. Simulations were carried out with one insertion with $c_0^{\text{ins}} = 0.1 \text{ nm}^{-1}$, $\kappa = 20 k_B T$, $\mu_V = 83.4 \text{ pN/nm}^2$.

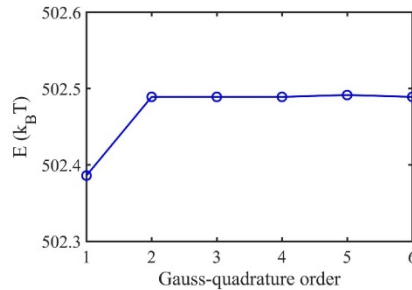


Figure S10. Second-order Gauss-quadrature is sufficient to accurately integrate bending energies. The simulation is carried out on the vesicle of $R = 28 \text{ nm}$ with $c_0^{\text{ins}} = 0.1 \text{ nm}^{-1}$, $\kappa = 20 k_B T$, $\mu_V = 83.4 \text{ pN/nm}^2$ and $\mu_A = 250 \text{ pN/nm}$.

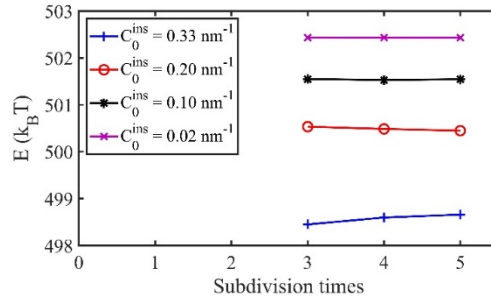


Figure S11. Energy calculations following insertion are not sensitive to the fineness of the triangular mesh beyond 3 subdivisions. The triangular mesh is generated by means of Loop's subdivision scheme. The more subdivision times give the finer mesh. Simulations here were carried out with the vesicle $R = 7$ nm and one insertion bound.

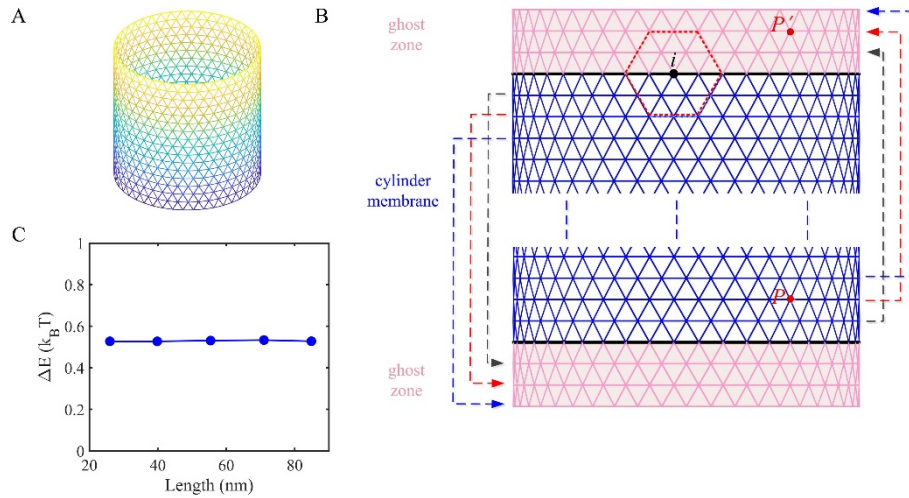


Figure S12. Cylinder membrane model. (A) A smooth triangular mesh for the cylinder membrane. (B) Ghost vertices and ghost faces (pink color). The cylinder (blue color) has two boundary ends (black solid line), which are constrained by periodic conditions. To apply the periodic condition, we introduce ghost vertices and faces beyond the cylinder boundary, and the ghost vertices or faces are three rows on each end to ensure that the nodal force on every boundary vertex is calculated sufficiently from all its neighbor faces. For example, in the figure, all the triangles inside the red dashed hexagon contribute to the nodal force of vertex i on the boundary, and thus three rows of ghost faces are sufficient. The periodic condition requires the two ends of the cylinder have the same neighborhood, which means the ghost vertex above the top of the cylinder should be translated from the cylinder bottom vertex, and the ghost vertex below the bottom of the cylinder should be translated from the cylinder top vertex, as shown by the dashed lines with arrows. For example, the position of ghost vertex P' is translated from the vertex P . To do so, we set the update of P' position is equal to the update of P position, $\Delta \vec{x}_{P'} = \Delta \vec{x}_P$. (C) The

energy change of the cylinder membrane following one insertion is not dependent on the cylinder length. Here, simulations were run with the bending modulus $\kappa = 20 k_B T$ and the insertion spontaneous curvature $c_0^{ins} = 0.35 \text{ nm}^{-1}$.